Retrieval of CO from nadir remote-sensing measurements in the infrared by use of four different inversion algorithms

Cathy Clerbaux, Juliette Hadji-Lazaro, Sébastien Payan, Claude Camy-Peyret, Jinxue Wang, David P. Edwards, and Ming Luo

Four inversion schemes based on various retrieval approaches (digital gas correlation, nonlinear least squares, global fit adjustment, and neural networks) developed to retrieve CO from nadir radiances measured by such downward-looking satelliteborne instruments as the Measurement of Pollution in the Troposphere (MOPITT), the Tropospheric Emission Spectrometer (TES), and the Infrared Atmospheric Sounding Interferometer (IASI) instruments were compared both for simulated cases and for atmospheric spectra recorded by the Interferometric Monitor for Greenhouse Gases (IMG). The sensitivity of the retrieved CO total column amount to properties that may affect the inversion accuracy (noise, ancillary temperature profile, and water-vapor content) was investigated. The CO column amounts for the simulated radiance spectra agreed within 4%, whereas larger discrepancies were obtained when atmospheric spectra recorded by the IMG instrument were analyzed. The assumed vertical temperature profile is shown to be a critical parameter for accurate CO retrieval. The instrument's line shape was also identified as a possible cause of disagreement among the results provided by the groups of scientists who are participating in this study. © 2002 Optical Society of America

OCIS codes: 010.1280, 010.7030, 280.1120, 300.6300, 300.6340.

1. Introduction

During recent decades the effects of human activities on the chemical composition of the atmosphere and climatic global warming have been subjects of increasing worldwide concern.[1,2] In the near future, satellite data will represent the majority of observations available for improving our understanding of global tropospheric chemistry. As a precursor of the production of ozone (O_3) and as the leading sink of hydroxyl radicals (OH), carbon monoxide (CO) is one of the key tropospheric trace species that need to be measured on a global scale. The primary emission sources of CO are associated with technological processes (transport, combustion, and industrial activities), biomass burning, biogenic sources, and oceans. Secondary sources come from the oxidation of methane (CH_4) and of nonmethane hydrocarbons. The estimated strengths of both natural and anthropogenic sources are uncertain to a great degree.[1] The chemical lifetime of CO varies from less than 1 month in the tropics to several months in the polar regions during winter, leading to large spatial and temporal variability of the CO global distribution. The analysis and interpretation of data measured by spaceborne nadir-looking instruments provide valuable information for study of CO sources, sinks, and transport processes.

The first CO tropospheric measurements from space were made by the Measurement of Air Pollution from Satellites (MAPS) instrument, a gas correlation spectrometer carried on board the Space Shuttle for limited time periods. CO retrievals were obtained for November 1981,[3] October 1984,[4] and April and October 1994.[5,6] Stratospheric and upper-tropospheric CO measurements were also provided from 26–31°N to 46–48°S by the Atmospheric Trace Molecular Spectroscopy (ATMOS) Fourier-transform

C. Clerbaux (ccl@aero.jussieu.fr) and J. Hadji-Lazaro are with Service d'Aéronomie, University of Paris 6, BP102, 4, Place Jussien, 75252 Paris, Cedex 5, France. S. Payan and C. Camy-Peyret are with the Laboratoire de Physique Moléculaire et Applications, University of Paris 6, BP102, 4, Place Jussien, 75252 Paris, Cedex 5, France. J. Wang and D. P. Edwards are with the National Center for Atmospheric Research, Atmospheric Chemistry Division, P.O. Box 3000, Boulder, Colorado 80307. M. Luo is with the Jet Propulsion Laboratory, 4800 Oak Grove Drive, Pasadena, California 91109.

Received 18 February 2002; revised manuscript received 1 July 2002.
0003-6935/02/337068-11$15.00/0

spectrometer during the Spacelab 3 Shuttle mission in May 1985.[7] The Interferometric Monitor for Greenhouse Gases (IMG) instrument flew aboard the Japanese Advanced Earth Observing System (ADEOS) from August 1996 to June 1997 and provided the first high-resolution (0.1-cm^{-1}) Fourier-transform infrared spectra in the nadir geometry.[8,9] More recently (December 1999), the Measurements of Pollution in the Troposphere (MOPITT) instrument[10] was launched as part of NASA's EOS–TERRA payload and has already given promising information on the tropospheric abundance of CO.[11,12]

Other nadir-viewing instruments that observe the spectrum of the Earth's atmosphere in the thermal infrared spectral range are planned for launch to probe the troposphere from polar-orbiting satellites. In the coming years, the Atmospheric InfraRed Sounder[13] (AIRS) will be launched on the U.S. EOS–AQUA platform, the Tropospheric Emission Spectrometer[14] (TES) is due to fly on EOS–AURA, and the Infrared Atmospheric Sounding Interferometer[15] (IASI) will be carried by the European METOP series of satellites. To maximize the scientific return from these missions, efforts are being dedicated toward the development of fast-forward radiative codes and efficient Level 2 (L2) inversion methods for the retrieval of infrared-absorbing trace species.

2. Methodology and Aims of the Intercomparison

Intercomparison experiments are needed to validate the information that can be measured from a remote-sensing instrument. Several *in situ* comparison campaigns that have gathered different kinds of instruments to measure atmospheric concentrations for several compounds at the same time and at the same geographical location have been organized.[16,17] Each instrument can use a different measurement technique, with associated software (the so-called retrieval algorithm) to extract the desired information (in this case atmospheric abundances of trace gases) from the raw data. A retrieval algorithm generally relies on a forward radiative transfer code, a spectroscopic database, and a minimization scheme.

As different nadir-sounding infrared instruments, all able to provide CO measurements on the global scale, potentially could fly during the same time period, we found it interesting to compare the L2 retrieval algorithms that were developed at the National Center for Atmospheric Research (NCAR) for the MOPITT instrument, at the Jet Propulsion Laboratory (JPL) for the TES, and at the Laboratoire de Physique Moléculaire et Applications (LPMA) and the Service d'Aéronomie (SA) in France for the IASI.

This paper is not intended as a comprehensive presentation of existing inversion methods but aims at comparing the performance of several inversion algorithms for a common set of data to quantify the level of agreement obtained when CO total column abundances are retrieved and to investigate possible causes of discrepancies. In 1999, high-resolution nadir radiance spectra measured in the thermal infrared spectral range were available from IMG measurements, allowing the four research teams who were developing the retrieval algorithms to test them on real atmospheric spectra. The algorithms used different forward radiative transfer codes and different minimization schemes but a common spectroscopic database.[18] As line-by-line forward radiative code intercomparison exercises had already been reported in the literature,[19,20] we focused on inversion codes that are specific to each instrument.

The inversion of geophysical parameters from remotely sensed observations is well known to be an ill-posed problem.[21] A variety of methods exists for the retrieval of atmospheric profiles from the spectra measured by remote sounders. A large body of literature is available on the subject,[22–24] and the approaches that are most widely used in atmospheric remote sensing have been described by Rodgers.[25] Retrievals of trace-gas and temperature profiles in the thermal infrared spectral range were reported for both simulation studies[26–28] and airborne experiments.[29,30] The accuracy of the retrieved quantities and the ability to retrieve low-resolution vertical profiles from the data provided by an instrument rely partly on the efficiency of the inversion procedure.

The L2 inversion codes used in this study are continually evolving to improve efficiency and performance. The 1999 version of each algorithm was used for this exercise, and data were not reprocessed with improved versions that have become available since then. All schemes were not at the same level of maturity at the time of our study, and some needed adaptation to be able to analyze IMG spectra. Each group was provided with a set of cloud-free IMG data. As an aid to analyzing the results, each research team was also provided with a set of synthetic spectra simulated by use of the IMG characteristics to investigate the effects of various properties that may affect the CO retrieval.

In this paper we summarize the results and discuss the agreement obtained for CO total column retrievals from a common data set. The paper is organized as follows: First, in Section 3 we briefly describe the inverse problem and the retrieval schemes that were used in the intercomparison exercise. Next, sensitivity studies to assess the performance of the four algorithms with regard to properties that may have an effect on the retrieval accuracy are reported, as well as CO inversion results from atmospheric spectra recorded by the IMG instrument (Section 4). In Section 5 we conclude with recommendations for improved CO retrievals for forthcoming instruments.

3. Retrieval Methods

A. Inverse Problem

The general remote-sensing equation can be written, in schematic form, as[25]

$$\mathbf{y} = \mathbf{F}(\mathbf{x}, \mathbf{b}) + \epsilon,$$

where $\mathbf{y}$ is the measurement vector (here the measured infrared radiances) and $\mathbf{F}(\mathbf{x}, \mathbf{b})$ is the forward model function. $\mathbf{x}$ is the state vector (here the CO

Table 1. Main Characteristics of the CO Retrieval Algorithms

Characteristic	Digital Gas Correlation (NCAR Team)	TWPR (JPL Team)	Global Fit (LPMA Team)	Neural Network (SA Team)
	Name of Algorithm			
Instruments	MOPITT[a]	TES[b]	IASI[c]	IASI
Forward codes	MOPFAS[d]	TWPR[e]	LPMA[f]	LBLRTM[g]
Atmospheric profiles	First guess	First guess	First guess	3D CTM[h]
Minimization algorithms	Maximum likelihood	Nonlinear least squares	Levenberg–Marquardt	Gradient descent
Spectral ranges (cm^{-1})	2100–2250	2000–2250	2000–2185	132 selected channels[i]
Presence of retrieved variables				
T_s/emissivity	x	x	x	
CO	x	x	x	x
H_2O			x	
Time required[j]	~1 s	>10 min	~10 min	<1 s

[a]Ref. 10.
[b]Ref. 14.
[c]Ref. 15.
[d]Ref. 31.
[e]Ref. 32.
[f]Ref. 33.
[g]Ref. 34.
[h]Ref. 35.
[i]Ref. 36.
[j]For one spectrum inversion in 1999 (not representative of the current performance of each algorithm).

concentration to be inferred from the measurement), and **b** represent all other components of the forward model: pressure, temperature, other constituent profiles, surface emissivity, instrument spectral function, and spectroscopic parameters. ε is the measurement error that is due to instrumental noise.

The inverse problem consists in retrieving **x** for a given **y.** For nadir-looking measurements, this problem is known to be nonlinear and underconstrained, as components of the atmospheric vertical profile do not contribute to the measurements and hence cannot be detected. The solution is nonunique and is generally unstable. As we mentioned in Section 2, different statistical and regularization techniques exist for deriving a valid solution,[25] allowing *a priori* knowledge or statistical (climatology) information to be taken into account.

B. Retrieval Schemes

The L2 inversion methods employed in this comparison exercise use different forward radiative codes, with different spectral ranges and minimization algorithms for the CO retrieval. Associated computing speed is variable, according to the number of simultaneously retrieved species. A short description of each algorithm is provided here, and Table 1 summarizes their main characteristics. The reader is invited to read the referenced publications for an extended description of each algorithm.

1. NCAR Inversion Algorithm

The MOPITT retrieval code is based on a parameterized fast-forward model[31] and uses maximum-likelihood inversion.[37] The digital gas correlation retrieval technique,[38,39] specifically developed to integrate observations made by various instruments (IMG, TES), was used for this intercomparison exercise. The simulated radiances and IMG spectra to be inverted were synthesized into MOPITT-like signals (thermal channels only) by filtering of the spectra with the MOPITT instrument function.[40]

2. JPL Inversion Algorithm

The JPL TES Working Prototype Retrieval (TWPR) algorithm, developed by the TES science team for TES L2 retrievals, is described in the TES Level2 Algorithm Theoretical Basis Document.[32] The general retrieval approach is to use nonlinear least-squares spectral fitting based on the so-called optimal estimation technique.[25] For computational efficiency, a table of lookup absorption coefficients at predefined pressure and temperature sets, and analytical Jacobian calculation, are used in the forward model. The code can accommodate both profile and column abundance retrievals.[41]

3. LPMA Inversion Algorithm

The LPMA retrieval algorithm is composed of an accurate radiative transfer model and an efficient minimization algorithm of the Levenberg–Marquardt type.[33] A global fit method[42] is used that permits simultaneous retrieval of the column amounts of more than eight species, surface temperature, surface emissivity, and instrumental spectral response function from a radiance spectrum. For the present research, the algorithm was tailored to the specifics of the IMG spectra and geometry.[43]

4. SA Inversion Algorithm

The SA retrieval scheme is based on a multilayer neural network that uses a gradient descent back-propagation algorithm.[43,44] Neural network tech-

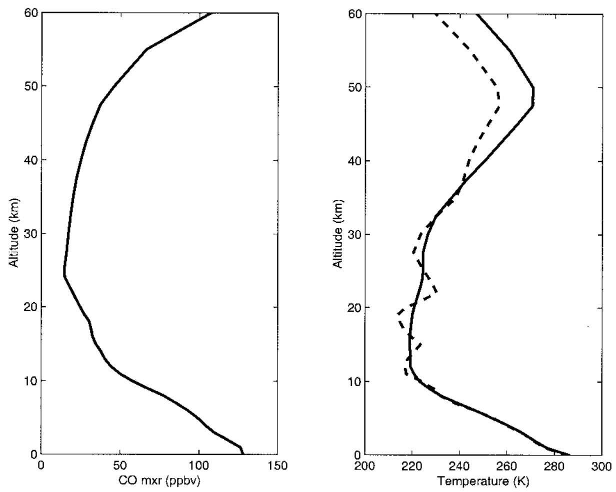

Fig. 1. CO mixing ratio (total column amount, 1.86×10^{18} molecules/cm^2) and temperature profiles used for the simulations. Solid and dashed curves, initial temperature profile and perturbed temperature profile, respectively. CO mxr (ppbv), CO mixing ratio, parts in 10^9 by volume.

niques permit the solution of regression problems by estimating a transfer function from a set of known situations that constitutes the *a priori* information that is necessary for solution of the problem. The database that was used to train the network was built from atmospheric concentration profiles calculated by a three-dimensional chemical-transport model[35] coupled to a radiative transfer code and convoluted with the desired instrumental function.[36]

4. CO Inversion

A. Simulated Radiance Spectra

Preliminary results obtained from comparison of the CO retrieval performance by use of the NCAR, LPMA, and SA codes on infrared nadir spectra were reported previously.[45] Concurrently with the analysis of CO inversion from the IMG atmospheric spectra, it was found necessary to perform sensitivity studies on simulations of IMG data, to study how errors associated with other parameters could propagate in the retrieved CO column amount. The spectrum of infrared radiation emitted by the Earth's surface and absorbed by the atmosphere as recorded by the IMG instrument in the nadir geometry was calculated with a high-resolution line-by-line radiative transfer code[34] with the HITRAN96 spectroscopic database.[18] CO concentration and temperature profiles (plotted in Fig. 1) extracted from the three-dimensional chemistry-transport Model for Ozone and Related Chemical Tracers[46,47] (MOZART) simulations above the North Atlantic Ocean (50°N, 25°E) for summer conditions were used as input. U.S. Air Force Geophysics Laboratory U.S. Standard Atmosphere 1976 concentration profiles were used for other absorbing species (H_2O, N_2O, O_3, and CH_4). Surface emissivity was set to 1. Solar ground reflection was not included in the calculation. The upwelling radiances were calculated on 48 fixed altitude levels from surface to 120 km. The high-resolution (5×10^{-4} cm^{-1}) spectrum calculated from 2000 to 2500 cm^{-1} was then resampled and convoluted to simulate IMG Level 1C radiance channels. The spectral dispersion of IMG in the CO absorption spectral range was set to 0.040177 cm^{-1}. As the exact IMG instrument line shape was unavailable, we used a Norton–Beer weak apodization function (full width at half-maximum, 0.06909 cm^{-1}), as our investigations showed that the unapodized IMG Level 1C data near 2100 cm^{-1} can be reasonably well fitted with this function.[48] Figure 2 (top) illustrates the radiative transfer simulation for IMG conditions, which is used hereafter as the reference (unperturbed) case. This radiance spectrum contains intense absorption features that are due to rovibrational transition lines of the 1–0 CO fundamental band from 2030 to 2230 cm^{-1}, with well-resolved lines associated with the *R* and *P* branches (Fig. 2, bottom). Interference occurs with the absorption features of H_2O, CO_2, O_3, and N_2O.

As described in Section 2, radiance recorded by an infrared nadir-looking instrument is a function of trace-gas concentration, atmospheric temperature profile, surface emissivity, and instrumental characteristics (noise and resolution). Other factors such as clouds and aerosols may also affect the measurement. For cloud-free conditions, most of the uncer-

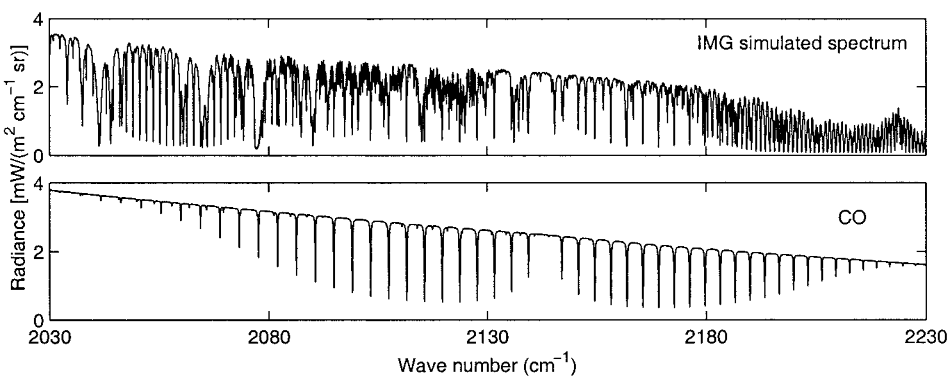

Fig. 2. Nadir radiance (reference) spectrum simulated at 0.07-cm^{-1} spectral resolution in the CO absorption spectral range for atmospheric conditions (top) and for CO alone (bottom).

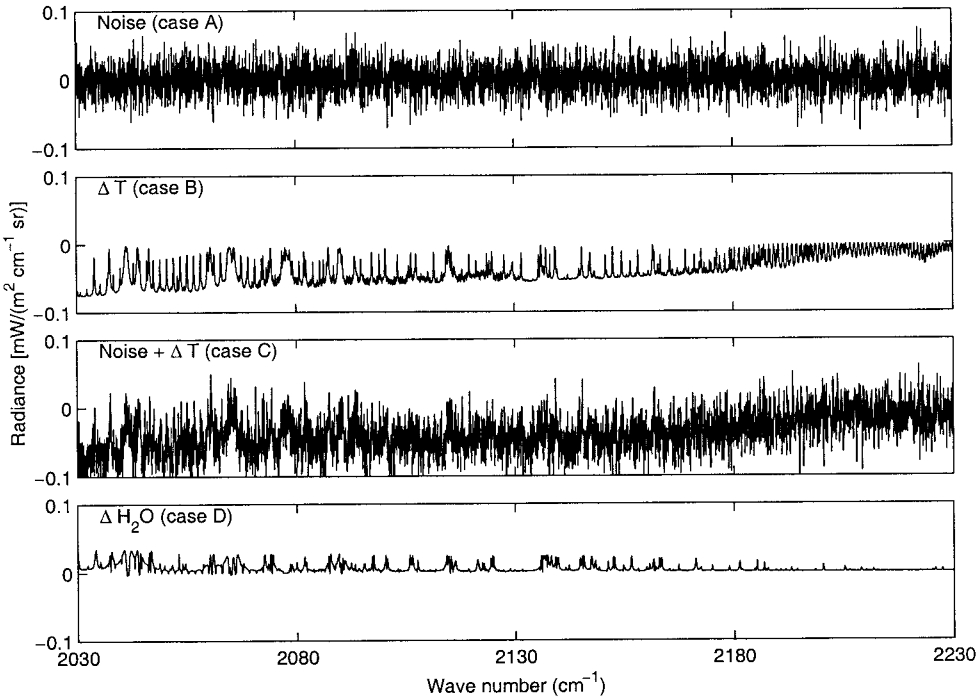

Fig. 3. Radiance differences from the initial reference spectrum: case A is for noise added; case B corresponds to a perturbed temperature profile; case C combines the addition of noise and the temperature perturbation; case D corresponds to a perturbed water-vapor profile.

tainty in the retrieved quantities comes from the instrumental noise and from the use of a temperature or other constituent vertical profile that may be erroneous. The sensitivity of the retrieved CO total column to the following factors has then been investigated: (1) instrumental noise, (2) temperature profile, and (3) water-vapor content.

1. *Instrumental Noise*

To simulate the contribution of instrumental noise to the signal, the reference radiance spectrum was perturbed by use of a Gaussian random-number generator. The standard deviation of the noise level was set to 2×10^{-5} W/m^2 cm^{-1} sr, corresponding to the IMG-associated noise for the 2100-cm^{-1} spectral range.

2. *Temperature Profile*

Temperature profiles are usually retrieved from the rovibrational bands of CO_2 near 650–700 cm^{-1}. For the forthcoming high spectral resolution instruments, it is expected that temperature will be measured with an accuracy of 1 K (rms) at a vertical resolution of 1 km, at least in the lower troposphere. The use of an erroneous temperature profile in the inversion process directly affects retrieval accuracy.

To simulate a realistic erroneous temperature profile, we used an error covariance matrix provided by Météo-France that characterizes the accuracy associated with the retrieval of a temperature profile for the IASI instrument. A previous example of such a matrix, which contains both diagonal and off-diagonal elements, was provided by Clerbaux *et al.*[36]; see Fig. 6 in that paper. The initial temperature profile was randomly perturbed by use of this error covariance matrix. Both the initial and the perturbed temperature profiles are plotted in Fig. 1. Differences are ~0.5 K at surface level (T_s), 0.05–1 K from surface to 7 km, and 0.5–5 K from 7 to 18 km; they increase at higher altitudes.

3. *H_2O Profile*

H_2O is the main interfering constituent in the CO absorption spectral range, with numerous absorption lines spread throughout the spectrum. The interference that is due to other constituents (N_2O, CO_2, and O_3) is easier to get rid of by careful selection of the microwindows used in the inversion process. To study how uncertainties in H_2O affect the signal, we applied a random perturbation of 10% (which is the expected accuracy to be provided by forthcoming infrared sensors) to the initial H_2O profile.

4. *Results*

Four specific kinds of radiance simulation that combined these three sources of error were prepared. Radiance perturbations from the initial unperturbed reference case are plotted in Fig. 3: Cases A, B, C, and D are associated with the radiance that is due to noise perturbation, to temperature profile perturbation, to combined noise and temperature perturbation, and to H_2O perturbation, respectively. The reference spectrum and the four perturbed spectra were distributed to each participating group of researchers, along with the ancillary data (temperature and other constituent profiles) associated with the

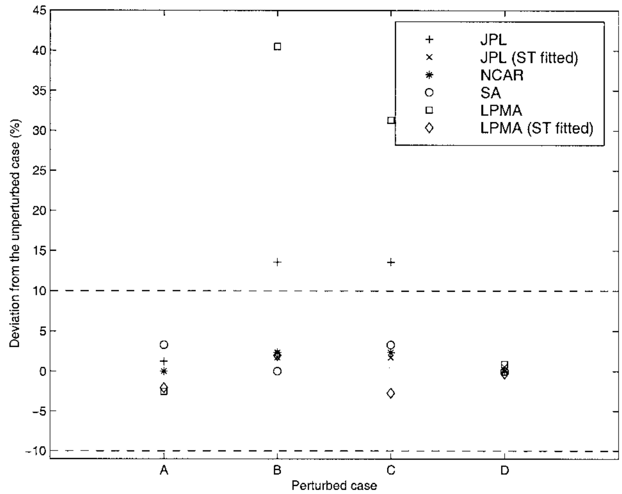

Fig. 4. Relative deviation for CO total column retrieval from the reference case for each participating research group (represented by symbols as shown). Case A is for noise added; case B corresponds to a perturbed temperature profile; case C combines the addition of noise and temperature perturbation; case D corresponds to a perturbed water vapor profile. Some results are provided with and without fitting of surface temperature (ST). The dashed horizontal line provides the standard accuracy expected for CO retrieval from infrared nadir radiances.

unperturbed reference case but without information on which specific parameter was investigated each time. The CO total column inversion results (CO_{inv}) obtained from the four groups are represented in Fig. 4. For the sake of clarity, and as this part of the exercise was focused on the study of how the various parameters affect the CO retrieved values, the results are plotted as relative deviations from the reference case (CO_{ref}), in percent: $(CO_{inv} - CO_{ref}) \times 100/CO_{ref}$. For each participant in the study, CO_{ref} corresponds to the CO amount retrieved from the unperturbed radiance spectrum. For JPL and for LPMA, two sets of results were provided for each case, one set with a fixed surface temperature at the value initially provided and a second set that allowed for the surface temperature to be adjusted by the fitting procedure. The results provided by NCAR were obtained with a fitted surface temperature. The SA algorithm is working with relative radiance values (baseline subtracted) to overcome the surface temperature adjustment.

In analyzing these results in detail, one can see that for all the research teams the addition of noise induced a small (null, slightly negative or positive, but always less than 4%) effect on the retrieved CO value (case A). The algorithms have different degrees of sensitivity when a different temperature profile from the one that was used to generate the spectrum (case B) is used in the inversion process. When the surface temperature parameter provided (which indeed differed by 0.5 K from the true surface temperature) was not adjusted by the fitting procedure, discrepancies of 40% could be reached. Conversely, when this parameter was allowed to be fitted, the agreement of CO retrievals among the four groups reached 3%. Case C, for which both noise (the same noise as used for case A) and a different temperature (the same as for case B) were combined, is consistent with the results obtained for these two cases. Finally, the use of a perturbed H_2O profile did not have a significant effect on retrieval for any of the groups (case D). In summary, when surface temperatures were allowed to be adjusted, relative agreement of better than 4% was found among all the codes for all four simulated cases that corresponded to perturbed situations. These differences are to be compared with the 10% accuracy value that is expected for the CO column amount retrieved from nadir infrared radiances. From this part of the comparison exercise we concluded that all four algorithms proved to be robust to noise and to retrieval errors caused by imperfect knowledge of temperature and H_2O profiles, at least for such reasonable noise levels and moderately perturbed profiles as those used for this part of the study.

B. IMG Radiance Spectra

1. *IMG Instrument*

The IMG instrument[8,9] operated on board the ADEOS satellite provided 10 months of data until breakdown of the platform's solar panel. IMG was a nadir-viewing Fourier-transform interferometer that recorded the thermal emission of the Earth-atmosphere system from 600 to 3030 cm^{-1}, with a maximum optical path difference of 10 cm. Owing to the polar orbit of the satellite, the instrument provided global coverage of the Earth, making 14.25 orbits per day with series of six successive measurements separated by 86 km along the track, followed by the observation of deep space and of an internal blackbody for calibration purposes. The footprint on the ground was 8 km $\times$ 8 km, in three spectral bands (band 1 from 2387 to 3030 cm^{-1}, band 2 from 2000 to 2500 cm^{-1}, and band 3 from 600 to 2000 cm^{-1}), corresponding to three different detectors and to three geographically adjacent footprints. The availability (through IMGDIS/ERSDAC) of the Level 1C atmospheric data recorded by the IMG instrument allowed us to compare our retrieval schemes with real atmospheric data.

2. *Results*

A set of five spectra (referred to hereafter as img304, img307, img822, img906, and img921), recorded at different places in the world and at different times of the year, was selected from the available IMG atmospheric data (version 5.5.2.3); each set of data had already been documented in previous papers as cloud-free data.[40,43,49] Table 2 summarizes the time and location for each IMG spectrum that was studied. The calibrated IMG Level 1C data are available with quality flags associated with three separate criteria: quality of the interferogram, quality of the alignment, and phase difference.[9] We verified that all

Table 2. IMG Spectra

Name of Spectrum	IMG File	Location Long.	Location Lat.	Day/Month/Year	h:min:s	Land or Sea	Elevation (m)
img307	432307	−52.3	41.0	16/06/97	01:40:01	Sea	0
img304	433304	60.1	24.5	16/06/97	18:24:33	Sea	0
img921	234921	−98.3	42.2	28/01/97	17:45:22	Land	575
img906	327906	9.5	38.4	03/04/97	21:36:00	Sea	0
img822	372822	27.0	37.3	05/05/97	09:19:14	Sea	0

five selected cases correspond to high-quality-flagged data.

Reliable temperature profiles, a key issue for the retrieval of accurate CO columns, are difficult to obtain, as can be seen from Fig. 5, which provides a set of temperature profiles that correspond to the location and time of spectrum img307. The three smooth profiles were calculated by meteorological models [the Arpege,[50] the European Centre for Medium-Range Weather Forecasts (ECMWF), the Japan Meteorological Agency (IMGDIS, IMG Level 2 data)]. The two other profiles, from Payan[51] and Serio[52], were directly retrieved from the IMG spectrum by use of the CO_2 absorption bands in IMG band 3.[49,53]

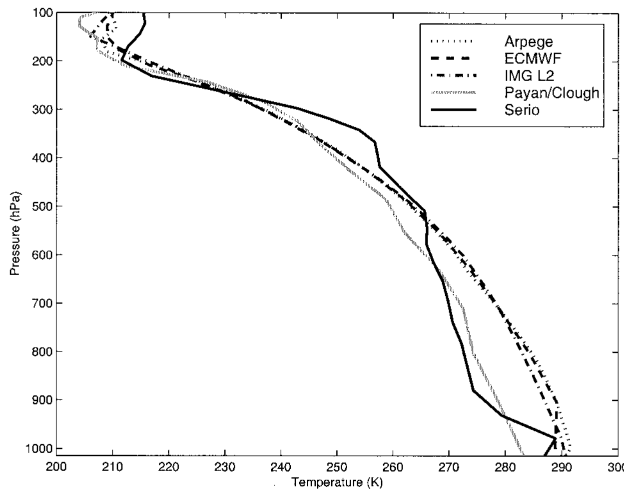

Fig. 5. Temperature profiles as provided by three meteorological (dashed curves) models and two retrieval (solid curves) algorithms for (−52.3° longitude, 41.0° latitude) on 16 June 1997 (01H40 UT).

The temperature profiles as retrieved by Serio *et al.*[52] were used in the inversion process to analyze the data, except for the img921 spectrum, referred to hereafter as the WINter Cloud Experiment (WINCE) for which colocated radiosonde H_2O and temperature profiles were available.[40] Figure 6 illustrates the good agreement obtained in the CO absorption spectral range between a Level1C IMG radiance spectrum (img307) and the adjusted spectrum calculated by the LPMA global fitting procedure. CO total column inversion results obtained from the participating groups are represented in Fig. 7. Again, results are provided as relative differences [here $100 \times (CO_{inv} - CO_{avg})/CO_{avg}$, where CO_{avg} is the mean value obtained from the averaging of all four results]. It can be seen that discrepancies can be large, ranging from a 17% difference between the two more distant results for the best-case agreement (img822) to 37% for the worst-case agreement (img906). The re-

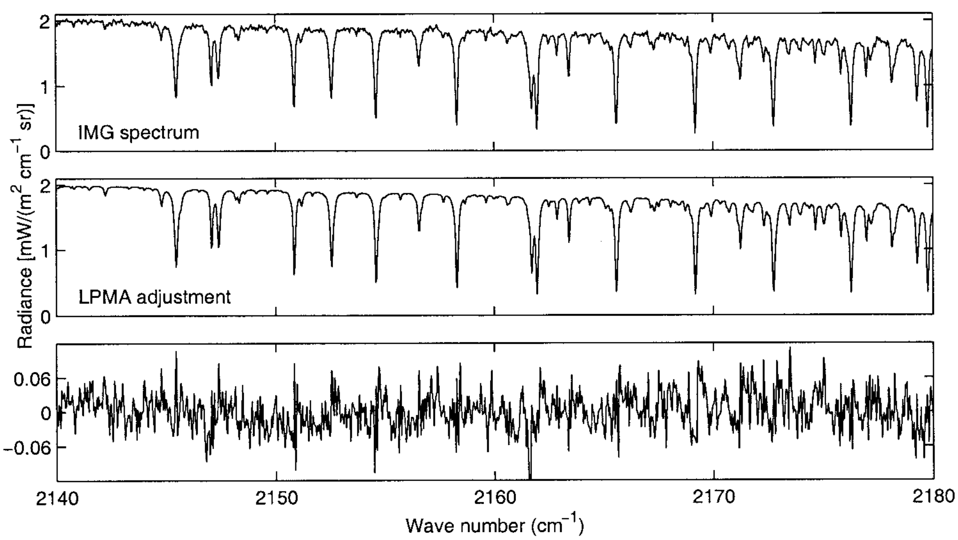

Fig. 6. IMG atmospheric spectrum, corresponding fit with the LPMA retrieval algorithm, and difference between these two spectra (bottom) in the CO absorption spectral range.

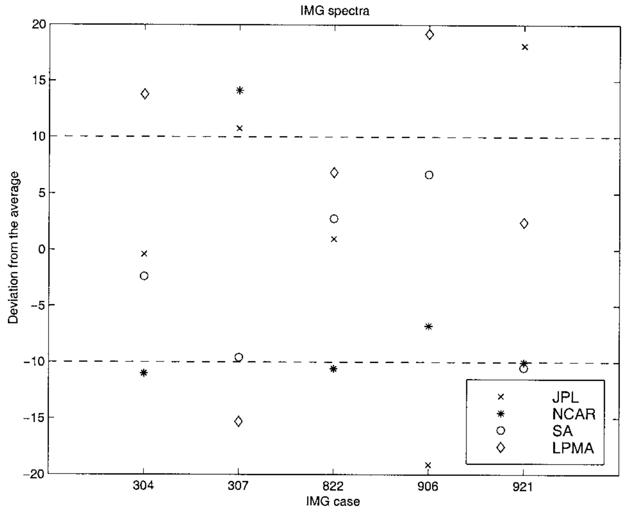

Fig. 7. Relative deviation for CO total columns from the averaged value as retrieved by the participating research groups using five selected IMG spectra. Averaged values (molecules/cm^2) are 1.50×10^{18}, 1.77×10^{18}, 1.64×10^{18}, 1.78×10^{18}, and 2.23×10^{18} for img304, img307, img822, img906, and img921, respectively (see Table 2 for recording times and locations). The dashed horizontal line provides the standard accuracy expected for CO retrieval from infrared nadir radiances.

sults obtained on simulated spectra from the first part of this exercise were used to analyze these discrepancies. Of the three properties (noise, temperature profile, and water-vapor content) that we perturbed so we could check their associated effects on the retrieval accuracy, only the temperature profile was found to be less easily determined than what was used for the simulated spectra. Also, as was already highlighted in some of the papers cited above, one of the major difficulties in the analysis of the IMG spectra is the lack of available information on the instrument line shape and ancillary geophysical parameters that are needed to invert CO, such as accurate colocated temperature profiles and information on cloud coverage.[43,49,54] These three sources of error were investigated.

3. *Temperature Profile*

Specific tests were performed with the LPMA retrieval algorithm on the img307 spectrum, fed with different temperature profiles (i.e., the profiles provided in Fig. 5). We found that differences between the CO columns obtained from the same algorithm and with different temperature profiles can reach 25%. In all cases, the algorithms that can adjust the surface temperature parameter to eventually compensate for an unknown surface emissivity, surface temperature, or both were allowed to fit this parameter. Discrepancies of a few degrees Kelvin between the initial surface temperature (provided by the first level of retrieved temperature profile) and the fitted value were found; they reached 10 K for img304.

4. *Instrument Line Shape*

We used the LPMA algorithm to perform various simulations to assess the effect of incomplete knowledge of the instrument line shape on retrieved CO column amounts. Several retrievals were performed with different instrument line shapes, and the relative differences between the retrieved CO columns reached 18%. As each algorithm uses its own spectral range and minimization scheme, the result of an incorrect instrument line shape for IMG data analysis is variable.

5. *Cloud Cover*

Another source of discrepancy could come from cloud coverage. Temperatures were retrieved with IMG band 3 data (where CO_2 absorption bands occur), whereas CO retrievals were obtained in band 2, where lines of the 1–0 fundamental transition occur. These two bands correspond to two adjacent footprints, separated by 12 km. Therefore, one pixel may be affected by the presence of cloud and the other not, result that affects either the temperature profile or the CO retrieval concentration. All the IMG band 2 cases studied were documented in previous studies as being cloud free in the CO spectral range.[40,49,54] But at least the band 3 corresponding pixel for img307 was identified as "possibly cloudy."[52]

5. Conclusions

The forthcoming launch of polar-orbiting and geostationary spacecraft with instruments that will sound the troposphere will greatly enlarge our knowledge and understanding of the global CO distribution, a key compound with which to investigate the tropospheric oxidation budget. Modern remote sounders are expected to provide CO column amounts with at least 10% accuracy, and possibly valuable vertical profiles with the help of data assimilation techniques.[55,56] The analysis of the radiance thermal channels provided by the IMG instrument on ADEOS,[44,56] and by the MOPITT instrument currently flying on EOS–TERRA, has already demonstrated the usefulness of nadir infrared soundings for the study of CO on the global scale.

In this paper we have examined four L2 inversion algorithms that are currently under development for the inversion of CO total columns from nadir upwelling radiances provided by the MOPITT, TES, and IASI instruments. This exercise generated useful interactions among the teams involved, to share experience and discuss specific problems, allowing us to improve our algorithms. Among other issues, we examined the channels used for the CO retrieval, the way the shape of the first-guess profile is modified in the adjustment procedure, and the effect of inaccurate surface temperature and emissivity parameters. We have tried to show that all four algorithms performed well on simulated radiance when ancillary data such as instrumental noise, temperature profile, and water-vapor content are known with a reasonable accuracy. The accuracy of 1 K/1 km in the troposphere, which should be reached for temperature profiles retrieved with the TES and IASI instruments, was shown to be adequate for accurate CO retrievals.

This exercise was also useful in making us aware of unexpected difficulties in the analysis of real atmospheric data. When data recorded by the IMG instrument were analyzed, the discrepancies among the inversion results increased and proved to be much more difficult to analyze. Divergences were attributed to a lack of information regarding the IMG instrument's line shape, to difficulty in using pixels that may exhibit different degrees of cloudiness for temperature and CO retrieval, and to unavailability of accurate temperature profiles. The IMG team is working on improvement of the instrument's line shape.[57] For current analyses of IMG data we recommend convolving the IMG spectra with an apodization function to overcome this problem (e.g., a Norton–Beer weak apodization function of 0.1 cm^{-1} FWHM for band 2).

Accurate trace-gas retrievals rely first on efficient forward radiative transfer codes and associated spectroscopic parameters, which are continually improved through the spectroscopic databases used worldwide. Second, well-defined instrumental characteristics (noise, instrument line shape) are needed. Third, reliable ancillary parameters (temperature, other gas profiles, cloud contamination) are also required. For both the TES and IASI missions, coincident improved retrievals of temperature (surface and atmospheric profile) and cloud coverage information should be available from the same instrument and within the same field of view as those used for the CO retrieval, which should minimize the propagation of incorrect determinations of these parameters in the CO retrieval.

Large amounts of new data will become available from upcoming satellite missions. To fully exploit the atmospheric data to be provided by different kinds of instruments, the scientific community should combine those data sets, e.g., to discover trends and global change issues.[58] Each instrument team is developing its own algorithm, adapted to each instrument's constraints and design. This exercise was a first step toward the analysis of a common set of infrared nadir radiances. The data set that was generated for this study is available on request (ccl@aero.jussieu.fr). We are continuing to refine each retrieval scheme, e.g., to retrieve CO vertical profiles and other trace gases such as O_3 and CH_4.[41,59]

The authors are very grateful to IMGDIS/ERSDAC for making the Level 1C IMG data available to us. We thank C. Serio for providing temperature profiles used in this study, P. Prunet for providing the IASI temperature error covariance matrix, and F. Karcher (Météo-France) for the Arpege temperature profile. We acknowledge valuable comments on this manuscript from A. Goldman, B. Sen, and two anonymous reviewers. This study was undertaken in the framework of the IASI Sounding Science Working Group (ISSWG) activities under the auspices of the European Organisation for the Exploitation of Meteorological Satellites and the Centre National d'Etudes Spatiales (France). NCAR is sponsored by the National Science Foundation.

References

1. World Meteorological Organization, *Global Ozone Research and Monitoring Project, Scientific Assessment of Ozone Depletion: 1998* (World Meteorological Organization, Geneva, 1997), Vol. 44.
2. J. T. Houghton, Y. Ding, D. J. Griggs, M. Noguer, P. J. van der Linden, X. Dai, K. Maskell, and C. Maskell, eds., *Climate Change 2001: The Scientific Basis,* contribution of Working Group I to the third assessment report of the Intergovernmental Panel on Climate Change (Cambridge U. Press, Cambridge, 2001).
3. H. G. Reichle, Jr., V. S. Connors, J. A. Holland, W. D. Hypes, H. A. Wallio, J. C. Casas, B. B. Gormsen, M. S. Saylor, and W. D. Hesketh, "Middle and upper tropospheric carbon monoxide mixing ratios as measured by a satellite-borne remote sensor during November 1981," J. Geophys. Res. D **91** 10,865–10,887 (1986).
4. H. G. Reichle, Jr., V. S. Connors, J. A. Holland, R. T. Sherrill, H. A. Wallio, J. C. Casas, E. P. Condon, B. B. Gormsen, and W. Seiler, "The distribution of middle tropospheric carbon monoxide during early October 1984," J. Geophys. Res. D **95,** 9845–9856 (1990).
5. V. S. Connors, B. B. Gormsen, S. Nolf, and H. G. Reichle, Jr., "Spaceborne observations of the global distribution of carbon monoxide in the middle troposphere during April and October 1994," J. Geophys. Res. D **104,** 21,455–21,470 (1999).
6. H. G. Reichle, Jr., B. E. Anderson, V. S. Connors, T. C. Denkins, D. A. Forbes, B. B. Gormsen, R. L. Langenfelds, D. O. Neil, S. R. Nolf, P. C. Novelli, N. S. Pougatchev, M. M. Roell, and L. P. Steele, "Space shuttle based global CO measurements during April and October 1994, MAPS instrument, data reduction and data validation," J. Geophys. Res. D **104,** 21,443–21,454 (1999).
7. C. P. Rinsland, M. R. Gunson, R. Zander, and M. Lopez-Puertas, "Middle and upper atmosphere pressure–temperature profiles and the abundances of CO_2 and CO in the upper atmosphere from ATMOS/Spacelab 3 observations," J. Geophys. Res. D **97,** 20,479–20,495 (1992).
8. H. Kobayashi, A. Shimota, K. Kondo, E. Okumura, Y. Kameda, H. Shimoda, and T. Ogawa, "A high-throughput Fourier-transform infrared radiometer for nadir Earth observations," Appl. Opt. **38,** 6801–6807 (1999).
9. H. Kobayashi, A. Shimota, C. Yoshigahara, I. Yoshida, Y. Uehara, and K. Kondo, "Satellite-borne high-resolution FTIR for lower atmosphere sounding and its evaluation," IEEE Trans. Geosci. Remote Sens. **37,** 1496–1507 (1999).
10. J. R. Drummond and G. S. Mand, "The measurement of pollution in the troposphere," J. Atmos. Oceanic Technol. **13,** 314–320 (1996).
11. D. P. Edwards, J.-L. Attié, J.-F. Lamarque, D. Ziskin, J. C. Gille, B. Khattatov, M. Deeter, M. Smith, J. Warner, G. L. Francis, C. Cavanaugh, L. Mayer, J. Chen, J. Drummond, G. Mand, and Z. Yu, "MOPITT observations of enhanced CO concentrations over Africa due to biomass burning," presented at the American Geophysical Union's 2000 Fall Meeting, San Francisco, Calif., 15–19 December 2000.
12. J.-L. Attié, J. Gille, M. Deeter, D. P. Edwards, B. Katthatov, J.-F. Lamarque, L. V. Lyjak, P. Novelli, M. W. Smith, J. Warner, and D. Ziskin, "Validation of CO retrievals from MOPITT instrument aboard Terra satellite, presented at the Eu-

ropean Geophysical Society Conference, Nice, France, 25–30 March 2001.

13. H. H. Aumann and C. Miller, "Atmospheric infrared sounder (AIRS) on the Earth Observing System," in *Advanced and Next-Generation Satellites,* H. Fujisaka and N. M. Sweeting, eds., Proc. SPIE **2583,** 332–338 (1995).
14. R. Beer, T. A. Glavich, and D. M. Rider, "Tropospheric emission spectrometer for the Earth Observing System's Aura satellite," Appl. Opt. **40,** 2356–2367 (2001).
15. F. Cayla and P. Javelle, "IASI instrument overview," in *Advanced and Next-Generation Satellites,* H. Fujisaka and N. M. Sweeting, eds., Proc. SPIE **2583,** 271–281 (1995).
16. C. Camy-Peyret, B. Bergquist, B. Galle, M. Carleer, C. Clerbaux, R. Colin, C. Fayt, F. Goutail, M. Nunes-Pinharanda, J. P. Pommereau, M. Hausmann, U. Platt, I. Pundt, T. Rudolph, C. Hermans, P. C. Simon, A. C. Vandaele, J. M. C. Plane, and N. Smith, "Intercomparison of instruments for tropospheric measurements using differential optical absorption spectroscopy," J. Atmos. Chem. **23,** 51–80 (1996).
17. A. Goldman, C. Paton-Walsh, W. Bell, G. C. Toon, J.-F. Blavier, B. Sen, M. T. Coffey, J. W. Hannigan, and W. G. Mankin, "Network for the detection of stratospheric change Fourier transform infrared intercomparison at Table Mountain facility, November 1996," J. Geophys. Res. D **104,** 30,481–30,503 (1999).
18. L. S. Rothman, C. P. Rindsland, A. Golman, S. T. Massie, D. P. Edwards, J.-M. Flaud, A. Perrin, C. Camy-Peyret, V. Dana, J.-Y. Mandin, J. Schroeder, A. McCann, R. R. Gamache, R. B. Wattson, K. Yoshino, K. V. Chance, K. W. Jucks, L. R. Brown, V. Nemtchinov, and P. Varanasi, "The HITRAN molecular spectroscopic database and HAWKS: 1996 edition," J. Quant. Spectrosc. Radiat. Transfer **60,** 665–710 (1998).
19. R. G. Ellingson and Y. Fouquart, "The intercomparison of radiation codes in climate models: an overview," J. Geophys. Res. D **96,** 8925–8927 (1991).
20. S. A. Tjemkes, T. Patterson, R. Rizzi, M. W. Shephard, S. A. Clough, M. Matricardi, J. Haigh, M. Höpfner, S. Payan, A. Trotsenko, N. Scott, P. Rayer, J. Taylor, C. Clerbaux, L. L. Strow, S. DeSouza-Machado, D. Tobin, and R. Knuteson, "ISSWG line-by-line intercomparison experiment," J. Quant. Spectrosc. Radiat. Transfer (to be published).
21. C. D. Rodgers, "Retrieval of atmospheric temperature and composition from remote measurements of thermal radiation," Rev. Geophys. **14,** 609–624 (1976).
22. U. Amato, I. De Feis, and C. Serio, "Linearization pseudo-noise and its effect on the retrieval of atmospheric state from infrared spectral radiances," Geophys. Res. Lett. **23,** 2565–2568 (1996).
23. B. Schimpf and F. Schreier, "Robust and efficient inversion of vertical sounding atmospheric high-resolution spectra by means of regularization," J. Geophys. Res. D **102,** 16,037–16,055 (1997).
24. P. Eriksson, "Analysis and comparison of two linear regularization methods for passive atmospheric observations," J. Geophys. Res. D **105,** 18,157–18,167 (2000).
25. C. D. Rodgers, Inverse Methods for Atmospheric Sounding: Theory and Practice, Vol. 2 of Series on Atmospheric, Oceanic and Planetary Physics (World Scientific, Singapore, 2000).
26. M. T. Chahine, "Inverse problems in radiative transfer: a determination of atmospheric parameters," J. Atmos. Sci. **27,** 960–967 (1970).
27. W. L. Smith, H. M. Woolf, and H. E. Revercomb, "Linear simultaneous solution for temperature and absorbing constituent profiles from radiance spectra," Appl. Opt. **30,** 1117–1123 (1991).
28. S. A. Clough, C. P. Rinsland, and P. D. Brown, "Retrieval of tropospheric ozone from simulations of nadir spectral radiances as observed from space," J. Geophys. Res. D **100,** 16,579–16,593 (1995).
29. W. W. McMillan, L. L. Strow, B. G. Doddridge, W. L. Smith, H. E. Revercomb, and H. L. Huang, "Retrieval of carbon monoxide column densities using AIRS on EOS: validation of a prototype retrieval algorithm," in *Optical Spectroscopic Techniques and Instrumentation for Atmospheric and Space Research II,* P. B. Hays and J. Wang, eds., **2830,** 169–179 (1996).
30. H. Worden, R. Beer, and C. Rindsland, "Airborne infrared spectroscopy of 1994 western wildfires," J. Geophys. Res. D **102,** 1287–1299 (1997).
31. D. P. Edwards, C. M. Halvorson, and J. C. Gille, "Radiative transfer modeling for the EOS Terra satellite Measurement of Pollution in the Troposphere (MOPITT) instrument," J. Geophys. Res. D **104,** 16,755–16,775 (1999).
32. Jet Propulsion Laboratory, "Level 2 algorithm theoretical basis document," Rep. JPL D-16474 (Jet Propulsion Laboratory, Pasadena, Calif., 1999); http://tes.jpl.nasa.gov/.
33. S. Payan, C. Camy-Peyret, P. Jeseck, T. Hawat, G. Durry, and F. Lefevre, "First direct simultaneous HCl and $ClONO_2$ profile measurements in the Arctic vortex," Geophys. Res. Lett. **25,** 2663–2666 (1998).
34. S. A. Clough and M. J. Iacono, "Line-by-line calculation of atmospheric fluxes and cooling rates. 2. Application to carbon dioxide, ozone, methane, nitrous oxide, and the halocarbons," J. Geophys. Res. D **100,** 16,519–16,535 (1995).
35. J.-F. Müller and G. Brasseur, "IMAGES: a three-dimensional chemical transport model of the global troposphere," J. Geophys. Res. D **100,** 16,445–16,490 (1994).
36. C. Clerbaux, P. Chazette, J. Hadji-Lazaro, G. Mégie, J.-F. Müller, and S. A. Clough, "Remote sensing of CO, CH_4, and O_3 using a space-borne nadir-viewing interferometer," J. Geophys. Res. D **103,** 18,999–19,013 (1998).
37. L. Pan, J. C. Gille, D. P. Edwards, P. L. Bailey, and C. D. Rodgers, "Retrieval of tropospheric monoxide for the MOPITT experiment," J. Geophys. Res. D **103,** 32,277–32,290 (1998).
38. J. Wang, J. C. Gille, P. L. Bailey, L. Pan, D. Edwards, and J. R. Drummond, "Retrieval of tropospheric carbon monoxide profiles from high-resolution interferometer Observations: A new digital gas correlation (DGC) method and applications," J. Atmos. Sci. **56,** 219–232 (1999).
39. J. Wang, J. C. Gille, P. L. Bailey, J. R. Drummond, and L. Pan, "Instrument sensitivity and error analysis for the remote sensing of tropospheric carbon monoxide by MOPITT," J. Atmos. Ocean. Technol. **16,** 465–474 (1999).
40. J. Wang, J. Gille, H. Revercomb, and V. Walden, "Validation study of the MOPITT retrieval algorithm: carbon monoxide retrieval from IMG observations during WINCE," J. Atmos. Oceanic Technol. **17,** 1285–1295 (2000).
41. M. Luo, R. Beer, D. J. Jacob, J. A. Logan, and C. D. Rodgers, "Simulated observation of tropospheric ozone and CO with the Tropospheric Emission Spectrometer (TES) satellite instrument," J. Geophys. Res. D 10.1029/2001JD000804 (2002).
42. M. Carlotti, "Global fit approach to the analysis of limb-scanning atmospheric measurements," Appl. Opt. **27,** 3250–3254 (1988).
43. C. Clerbaux, J. Hadji-Lazaro, S. Payan, C. Camy-Peyret, and G. Mégie, "Retrieval of CO columns from IMG/ADEOS spectra," IEEE Trans. Geosci. Remote Sens. **37,** 1657–1662 (1999).
44. J. Hadji-Lazaro, C. Clerbaux, and S. Thiria, "An inversion algorithm using neural network to retrieve atmospheric CO concentrations from high-resolution nadir radiances," J. Geophys. Res. D **104,** 23,841–23,854 (1999).
45. C. Clerbaux, J. Hadji-Lazaro, S. Payan, C. Camy Peyret, and J. Wang, "Intercomparison of inversion algorithms for the retrieval of CO from IMG/IASI, presented at the 8th International Workshop on Atmospheric Science from Space Using

Fourier Transform Spectrometry, Toulouse, France, 16–18 November 1998.
46. G. P. Brasseur, D. A. Hauglustaine, S. Walters, P. J. Rasch, J.-F. Müller, C. Granier, and X. X. Tie, "MOZART, a global chemical transport model for ozone and related chemical tracers. 1. Model description," J. Geophys. Res. D **103,** 28,265–28,289 (1998).
47. D. A. Hauglustaine, G. P. Brasseur, S. Walters, P. J. Rasch, J.-F. Müller, L. K. Emmons, and M. A. Carroll, "MOZART, a global chemical transport model or ozone and related chemical tracers. 2. Model results and evaluation," J. Geophys. Res. D **103,** 28,291–28,335 (1998).
48. S. Payan, Laboratoire de Physique Moléculaire et Applications, Paris, France, and J. Hadji-Lazaro, Service d'Aéronomie, Paris, France. (personal communication, 1998).
49. A. M. Lubrano, C. Serio, S. A. Clough, and H. Kobayashi, "Simultaneous inversion for temperature and water vapor from IMG radiances," Geophys. Res. Lett. **27,** 2533–2536 (2000).
50. F. Karcher, MétéoFrance, Toulouse, France (personal communication, 1998).
51. S. Payan, Laboratoire de Physique Moléculaire et Applications, Paris, France (personal communication, 1998).
52. C. Serio, Università di Basilicata, Potenza, Italy (personal communication, 1999).
53. U. Amato, V. Cuomo, I. De Feis, F. Romano, C. Serio, and H. Kobayashi, "Inverting for geophysical parameters from IMG radiances," IEEE Trans. Geosci. Remote Sens. **37,** 1620–1632 (1999).
54. J. Hadji-Lazaro, C. Clerbaux, P. Couvert, P. Chazette, and C. Boonne, "Cloud filter for CO retrieval from IMG infrared spectra using ECMWF temperatures and POLDER cloud data," Geophys. Res. Lett. **28,** 2397–2400 (2001).
55. J.-F. Lamarque, B. V. Khattatov, J. C. Gille, and G. P. Brasseur, "Assimilation of Measurement of Air Pollution from Space (MAPS) CO in a three-dimensional model," J. Geophys. Res. D **104,** 26,209–26,218 (1999).
56. C. Clerbaux, J. Hadji-Lazaro, D. Hauglustaine, G. Mégie, B. Khattatov, and J.-F. Lamarque, "Assimilation of carbon monoxide measured from satellite in a three-dimensional chemistry-transport model," J. Geophys. Res. D **106,** 15,385–15,394 (2001).
57. S. Ichizawa, K. Kondo, M. Suzuki, H. Shimoda, and T. Ogawa, "Improvement of the instrument line shape of IMG," in *Infrared Spaceborne Remote Sensing IX,* M. Strojnik and B. F. Andresen, eds., Proc. SPIE **4486,** 326–334 (2002).
58. J. E. Harries, H. E. Brindley, P. J. Sagoo, and R. J. Bantges, "Increases in greenhouse forcing inferred from outgoing long-wave radiation spectra of the Earth in 1970 and 1997," Nature **410,** 355–357 (2001).
59. S. Turquety, J. Hadji-Lazaro, and C. Clerbaux, "Retrieval of ozone from infrared IASI measurements," in *Remote Sensing of Clouds and the Atmosphere VI,* K. Schaefer, O. Lado-Bordowsky, A. Comeron, M. R. Carleer, and J. S. Fender, eds., Proc. SPIE **4539,** 106–115 (2002).